Zeitschrift für Medizinische Physik xxx (xxxx) xxx

Contents lists available at ScienceDirect

Zeitschrift für Medizinische Physik

journal homepage: www.elsevier.com/locate/zemedi

Original Paper

Multi-angle beam range measurement framework for carbon-ion radiotherapy using a commercial multi-layer ionization chamber

Soorim Han [a], YongCheol Kwon [a], Taegeon Oh [a], Eunho Lee [a], Eun Kyu Kim [a], Tae Ho Kim [b], Dohyeon Yoo [b], Sangmin Lee [b], Changhwan Kim [b,*], Min Cheol Han [b,*], Chae-Seon Hong [b], Jin Sung Kim [b]

[a] Department of Radiation Oncology, Heavy Ion Therapy Research Institute, Yonsei Cancer Center, Yonsei University Health System, Seoul, the Republic of Korea
[b] Department of Radiation Oncology, Heavy Ion Therapy Research Institute, Yonsei Cancer Center, Yonsei University Health System, Yonsei University College of Medicine, Seoul, the Republic of Korea

ARTICLE INFO

Keywords:
Carbon-ion radiotherapy
Beam range measurement
Multi-layer ionization chamber
Gantry irradiation system
Qualityassurance

ABSTRACT

Accurate beam range verification is critical in carbon-ion radiotherapy, where the sharp Bragg peak and complex material-dependent nuclear interactions pose greater measurement challenges compared to proton therapy; however, conventional water phantom methods for frequent and comprehensive checks required for routine quality assurance (QA) are extremely time-consuming. This study proposes and validates a framework using a commercial multi-layer ionization chamber (MLIC) to enable efficient, accurate, and comprehensive range verification.

The framework integrates three key innovations: (1) a beam-model-based fitting method that uses reference integral depth-dose curves to reduce range determination uncertainty for carbon ions, (2) a time-optimized, trigger-free acquisition process, and (3) a custom gantry-compatible mount for stable multi-angle measurements. The framework's measurement uncertainty was evaluated via range-shift experiments, and its clinical feasibility was tested through year-long stability and multi-angle consistency measurements.

The proposed method demonstrated a low range-determination uncertainty, with an expanded uncertainty of 0.24 mm ($k = 3$), and showed excellent agreement with standard water phantom measurements (mean deviation of 0.03 ± 0.15 mm). The framework reduced the measurement time for all 600 energy levels from >50 h to approximately 15 min, representing >100-fold improvement. Clinical validation confirmed high stability, with long-term and multi-angle deviations of 0.17 mm and 0.05 mm ($k = 1$), respectively. The system also successfully identified machine-related beam range inconsistencies that were not detectable using conventional QA protocols.

The proposed MLIC-based framework provides a reliable, accurate, and highly efficient solution for routine beam range QA in carbon-ion therapy. Its successful clinical application demonstrates its feasibility for frequent and comprehensive verification across all energy levels and gantry angles.

Introduction

Carbon-ion radiotherapy (CIRT) is an advanced modality in cancer treatment that provides superior dose conformity and enhanced biological effectiveness compared with conventional photon therapy [1–3]. CIRT achieves the desired depth-dose distribution by modulating the energy of the incident beam. In clinical practice, the incident beam energy dictates its penetration depth in the material. This strong physical correlation is utilized for quality assurance (QA), where the beam range in water is measured as a key parameter to verify the stability and accuracy of the delivered energy.

The conventional beam range measurement method that uses a water phantom and ionization chamber is considered the gold standard for low-uncertainty tasks and is indispensable for initial commissioning. However, its labor-intensive and time-consuming point-by-point process makes it impractical for frequent and comprehensive checks required in routine QA. These limitations, particularly the difficulty of verifying hundreds of energies and the physical restrictions on gantry angle measurements, establish a clear need to have a more efficient approach for routine verification.

* Corresponding authors at: Heavy Ion Therapy Center, Yonsei Cancer Center, 50-1 Yonsei-ro, Seodaemun-gu, Seoul 03722, the Republic of Korea
E-mail addresses: chkim514@yuhs.ac (C. Kim), mchan@yuhs.ac (M.C. Han).

https://doi.org/10.1016/j.zemedi.2026.03.007
Received 23 November 2025; Accepted 9 March 2026

To overcome these limitations, several alternative approaches have been explored. Some solutions, such as compact water column phantoms, provide low-uncertainty, multi-angle measurements but do not resolve the time-inefficiency issue for comprehensive QA across all energy levels [4]. Other common approaches combine a two-dimensional (2D) array detector with a range shifter of position-dependent thickness (e.g., a wedge or a rotating cylindrical phantom) [5,6], but their scope is typically limited to verifying the range consistency of a few-sampled energies, and they are constrained by structural limitations that introduce considerable setup-dependent measurement uncertainty. The most promising approach for rapid verification is the multilayer ionization chamber (MLIC) [7], which offers a potential solution by enabling the instantaneous acquisition of a complete depth-dose distribution.

While the Giraffe MLIC system (IBA Dosimetry, Germany) demonstrates an approximate measurement uncertainty of 0.5 mm for proton beams [8,9], it has limitations when applied to carbon-ion beam range measurements. The vendor-provided analysis software (OmniPro Incline v1.1.2.0) primarily utilizes the Bortfeld model, an analytical approximation specifically designed for proton Bragg curves [10]. However, the Bragg curve of a carbon-ion beam differs fundamentally from that of a proton beam, exhibiting distinct characteristics, such as a considerably larger plateau-to-peak ratio, a narrower peak width due to energy straggling, and the presence of a fragmentation tail [11]. As the Bortfeld model does not accurately account for these unique characteristics of carbon-ion beams, its application leads to increased uncertainty and reduced reliability in range determination for carbon ions. Therefore, overcoming these limitations requires a new framework tailored for accurate and reliable range determination of carbon-ion beams. Furthermore, applying the Giraffe system for multi-angle QA on a gantry is impractical in its standard configuration, as the system is not supplied with a dedicated mount for stable setups at various angles, which effectively limits its routine use to vertical or horizontal beam orientations.

To address the previously mentioned limitations for routine QA, this study introduces and validates a novel framework designed for rapid, accurate, and comprehensive beam range verification. This MLIC-based framework integrates three key innovations to overcome the specific challenges of carbon-ion therapy: (1) a beam-model-based fitting method to ensure low measurement uncertainty, and (2) a time-optimized acquisition process that enables range verification for a vast number of energy conditions within a clinically practical timeframe. Additionally, for gantry-based systems, (3) a gantry-compatible mount was developed to extend these capabilities to stable measurements at any gantry angle.

This study presents a comprehensive evaluation of the proposed framework to validate its performance. The framework's performance was assessed by evaluating its range determination uncertainty and agreement with standard water phantom measurements. Furthermore, its clinical feasibility and utility were demonstrated through a year-long analysis of long-term range constancy and an extensive evaluation of range consistency across 12 gantry angles.

Methods

Heavy ion therapy facility

The Heavy Ion Therapy Center (HITC) at the Yonsei Cancer Center (YCC) is the first facility in South Korea to offer CIRT [12]. The YCC consists of three treatment rooms: one equipped with a fixed horizontal beam, and two equipped with rotating superconducting gantries [13], allowing beam delivery at various angles. The center utilizes a synchrotron-based scanning beam irradiation system [14,15] that supports lateral irradiation fields of up to 20 cm × 20 cm. The synchrotron provides 600 discrete energy levels ranging from 55.6 MeV/u to 430 MeV/u for generating Bragg peaks at water-equivalent depths in the range of 2–302 mm. Notably, the system supports a multiple-energy operation capable of rapid switching (0.4–0.85 s) among different beam energies within a single extraction spill, a feature that enables highly efficient sequential irradiation across the full set of energy levels [16].

This system combines the flexibility of the scanning system for lateral spot positioning with the precise distal positioning capabilities of the synchrotron [13], enabling the delivery of conformal three-dimensional (3D) dose distributions adapted to the geometry of the tumors. As the pristine Bragg peak exhibits a sharp distal penumbra unsuitable for these clinical applications, a ridge filter (RGF) was typically employed to broaden the peak to enhance the robustness of the dose distributions.

Standard beam-range measurement procedure

At YCC, the beam range is defined as R80—the depth in water on the distal fall-off where the dose falls to 80% of the maximum, measured with a 1 mm RGF in place [17]. This definition serves as the standard for all range measurements discussed herein.

For the initial commissioning of the treatment planning system (TPS), a set of reference data, commonly referred to as a "beam model," must be established. This one-time process involves measuring the complete integral depth-dose (IDD) curves —representing the depth dose distribution integrated over the entire beam spot area measured using large area detector— for a representative subset of beam energies (specifically, the 32 energies defined for beam modeling at YCC). As shown in Fig. 1(a), these measurements are performed using a large-area parallel-plane ionization chamber (ACLD, AEC, Chiba, Japan) in a large-scale 3D water phantom (100 × 77.5 × 175 cm; approximate weight of 220 kg when filled) to ensure the lowest uncertainty under reference conditions [18].

Acquiring a single high-resolution IDD curve is time-intensive (approximately 30 min per energy), leading to a total measurement time of >16 h for the 32 reference energies. The R80 values determined from these 32 measured IDDs serve as the gold-standard reference ranges for their respective energies. The TPS then utilizes these measured IDDs to generate the full library of 600 clinical beam profiles through an interpolation process [19]. This foundational dataset, once established, is used for all clinical treatment planning.

Distinct from one-time commissioning, routine QA aims to periodically verify the beam range stability. For this, measuring the full IDD is unnecessary; instead, a streamlined process is used to measure the range (R80) directly. This process, which is based on a water phantom and an ion chamber and will hereafter be referred to as the standard QA method, is achieved by taking approximately 10 measurements around the Bragg peak in a point-by-point fashion, where each point requires a sequence of detector movements, measurement initiation, data acquisition, readout, and reset, resulting in a total time of approximately 5 min per energy. Furthermore, this "stop-and-go" mechanical nature requires the detector to be stationary for each discrete energy measurement, rendering the standard QA method incompatible with any rapid, successive energy-switching sequence.

While this process is efficient for verifying a few energies, it becomes impractical for comprehensive QA across all available energy levels. A full 600-energy verification would still require more than 50 h of beam time, which is unfeasible for weekly, monthly, or even annual QA schedules. Consequently, current routine QA protocols are typically limited to the verification of a small subset of energies at regular intervals. This limitation creates a potential risk of failing to detect range deviations in the unmeasured majority of energies, establishing a clear need for a more rapid and comprehensive verification method.

The Proposed MLIC-Based Framework

MLIC

The MLIC is an advanced device designed for precise depth-dose

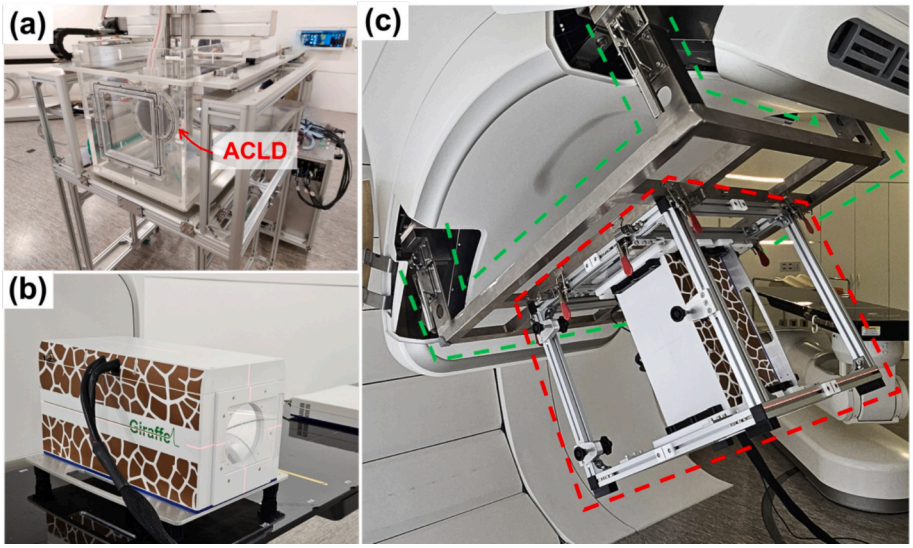

Fig. 1. Photographs of the devices used for the range measurements. (a) large-area parallel-plane ionization chamber with water phantom, (b) Giraffe, and (c) developed Giraffe mount (red line) attached to the gantry attachment (green line) at a gantry angle of 30°.

measurements in particle therapy. It comprises a stack of independent, air-vented, parallel-plane ionization chambers fabricated using printed-circuit-board technology. Structurally, each measurement layer is formed by an air gap sandwiched between the electrode plates. The PCB substrates of these electrodes simultaneously function as the absorber material. Consequently, the water-equivalent depth associated with each measurement channel corresponds to the cumulative water-equivalent thickness (WET) of the preceding substrate layers traversed by the beam. This stacked geometry enables efficient and simultaneous depth-dose measurements and considerably improves the workflow efficiency for beam-range assessments[20].

The Giraffe MLIC using IBA Dosimetry delivers reliable and accurate measurements (Fig. 1(b)). The system comprises 180 independent ionization chamber channels, each separated by an air gap with a water-equivalent thickness of approximately 1.9 mm/channel. The device features circular electrodes with a diameter of 12 cm to capture the scattered beam components. Simultaneous dose measurements across depths of 2–330 mm were obtained, providing comprehensive data for determining the beam range. The Giraffe MLIC weighs approximately 10 kg and has dimensions of 17.5 cm × 43.9 cm × 19.5 cm (Width (W) × Depth (D) × Height (H)), which makes it considerably smaller and lighter than the standard water phantom, and allows easier handling in practical settings.

For this study, the Giraffe detector was calibrated by following the vendor-recommended protocol using the facility's maximum energy carbon-ion beam (430 MeV/u). To ensure accurate channel-to-channel response and depth of each channel, the gain and spatial (depth) calibration procedure involved irradiating the detector from both the front and back directions. This method utilizes the low-gradient plateau region of the Bragg curve to determine the gain factor for each channel, ensuring the measured signal matches the physical dose distribution. Data acquisition was managed using the OmniPro software (version 1.1, IBA Dosimetry, Germany), which provides a built-in range analysis function based on the proton-optimized Bortfeld curve [10]. This analytical fitting provides a precise range determination that overcomes the physical resolution limitations of the detector. While this built-in range analysis yields low uncertainty for protons, with a reported mean deviation of only 0.1 ± 0.3 mm, its uncertainty is considerably higher for carbon ions (deviation of 0.2 ± 0.7 mm) owing to the distinct characteristics of their Bragg curves [9]. Therefore, to bypass this limitation, we utilized OmniPro's capability to export raw measurement data, specifically referring to the gain-calibrated signal values from all 180 individual channels. This raw data then served as the input for the new, more accurate analysis method developed in this study.

Range analysis with beam-model-based fitting

Although the Bortfeld approximation serves as the default fitting method used in the commercial software, OmniPro-Incline, it exhibits known limitations when applied to carbon ion beams [10,21]. To address these issues and improve range determination accuracy, we propose a data-driven fitting approach that utilizes a library of measured water IDD curves as practical reference templates. This approach utilizes the 32 reference IDD curves—originally acquired for TPS beam modeling using the ACLD and water phantom—as fitting templates to determine the range from the MLIC measurement data.

Admittedly, the material composition of the ACLD in water differs from the MLIC's multilayer PCB structure, which can affect the Bragg curve shape. Ideally, the reference templates should be derived from the specific detector response to carbon ions, considering the effective atomic number of materials and air gaps within the MLIC. However, accurate modeling of the commercial MLIC is constrained by the lack of public information regarding its detailed material composition and internal geometry. Furthermore, performing Monte Carlo simulations to generate detector-specific look-up tables requires precise modeling of the beam line components (e.g., RGF) and beam optics, which can vary significantly between institutions and introduce user-dependent uncertainties. Therefore, this study adopts a semi-empirical approach using measured water-based IDD curves as the reference templates. This method prioritizes practicality and reproducibility, providing a measurement-driven solution that does not rely on complex, institution-specific simulations or proprietary detector specifications.

As illustrated in Fig. 2, the process begins by selecting the reference IDD curve with a peak closest to that of the MLIC measurement (Fig. 2 (a)). This selected curve (IDD_{ref}) is then adjusted by applying a depth shift (Δd) and a dose scaling factor (α) to generate a fitted curve (IDD_{fit}). The optimal Δd and α values are determined by minimizing the root-mean-square difference between the fitted curve and the measured data over the region from the peak -8 mm to peak +4 mm (Fig. 2(b)). Finally, the range (R80) is determined from this optimally aligned fitted curve. The reliability of this approach was evaluated by comparing the resulting curves and ranges with those derived from Bortfeld fitting and spline interpolation.

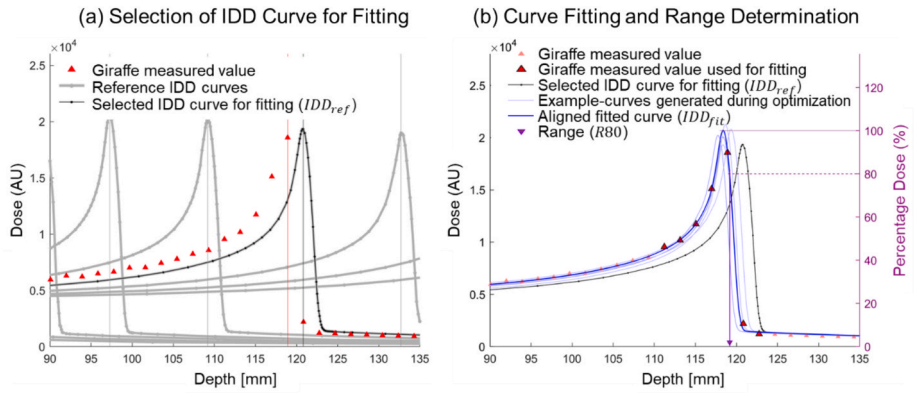

Fig. 2. Beam-model-based fitting process for range determination. (a) Selection of the reference integral depth-dose (IDD) curve closest to the measured multilayer ionization chamber (MLIC) peak. (b) Adjustment of the selected curve to align with MLIC data using depth shift and dose scaling. The R80 value was determined from the aligned fitted curve.

MLIC mount for gantry

In a gantry system that uses multiple angles for treatment, the measurement directions of the MLIC must be accurately aligned with those of the gantry system to perform beam-range measurements at various angles. To precisely determine the range at every angle, each measurement must be accurately positioned with the irradiation angle of the gantry.

To achieve this, an MLIC-specific mount was designed that was compatible with the gantry attachment used for the measurement devices provided by the CIRT system (Fig. 1(c)). The mount dimensions were 55 cm × 50 cm × 50 cm (W × D × H), and it weighed approximately 20 kg when combined with the Giraffe MLIC. To verify that the MLIC could be precisely set up at different angles without distortion owing to its weight, it was attached to the mount and rotated at 30° intervals. A digital spirit level was used to measure the MLIC angle at each gantry angle and confirm its alignment within ±0.1°.

Optimization of measurement process

While our accelerator's multiple-energy operation allows it to deliver all 600 discrete energy levels in approximately 15 min, the conventional measurement approach using the Giraffe—a sequential process that performs a separate irradiation run and data acquisition for each individual energy level—creates a major bottleneck, prolonging verification times to many hours. To overcome this bottleneck, we developed an optimized process that synchronizes the measurement time with the rapid beam delivery time.

Instead of a trigger-based method, we employed a continuous data acquisition approach followed by postprocessing to distinguish the data from each energy level. Using the "movie mode" of OmniPro, we recorded a continuous time series of dose data during a single irradiation run that cycled through all 600 energies. Importantly, the MLIC operates in current mode, where each measurement represents a macroscopic, time-averaged dose signal integrated over a specific sampling interval. In the subsequent analysis, the data points were assigned to their respective energy levels based on the magnitude of the measured signal. The feasibility of this approach is ensured by a carefully selected sampling time of 0.3 s; this interval is longer than the 0.1 s irradiation time but shorter than the 0.4 s minimum energy modulation time, effectively preventing signal pile-up.

This optimized process successfully reduces the entire measurement time to match the duration of the beam delivery process (~15-min), enabling rapid and comprehensive QA.

Validation of the proposed framework

The framework's measurement uncertainty was quantified using a range-shift experiment, and the agreement was evaluated by comparing the framework's results against the reference ranges established by the standard method. These experiment designs are described below.

Analysis of measurement uncertainty

To quantitatively evaluate the framework's intrinsic measurement uncertainty ($u_{intrinsic}$), a range-shift experiment was performed. For this analysis, measurements were made for 300 distinct beam energies under four conditions: a reference measurement without a slab and three subsequent measurements with 1-, 2-, and 4-mm water-equivalent RW3 slabs (PTW, Germany) placed immediately upstream of the MLIC, resulting in 1200 range measurements. The range-shift by the slab, ΔR, was then calculated for each slab using the equation:

$$\Delta R = R_{ref} - R_{mat}. \tag{1}$$

where R_{ref} is the range measured without the slab, and R_{mat} is the range with the slab.

The combined standard uncertainty, u_C, of the measured range-shift (ΔR) was evaluated by statistical analysis (Type A evaluation). It corresponds to the experimental standard deviation of the 300 ΔR values. Assuming the standard uncertainty of a single range measurement $u(R)$, is consistent regardless of the slab (i.e., $u(R_{ref}) \approx u(R_{mat}) \approx u_{intrinsic}$), the relationship follows the law of propagation of uncertainty:

$$u_C^2 = u(R_{ref})^2 + u(R_{mat})^2 \approx 2 \cdot u_{intrinsic}^2. \tag{2}$$

Thus, the range measurement uncertainty, $u_{intrinsic}$, was derived as:

$$u_{intrinsic} = \frac{u_c}{\sqrt{2}} \tag{3}$$

This procedure was applied to all three fitting methods to compare their intrinsic uncertainty quantitatively.

Agreement assessment with reference standard

The agreement of the framework was validated in two ways. The primary assessment involved the comparison of the ranges derived from the MLIC for the 32 reference energies against their corresponding gold-standard values. As the framework is not calibrated to each individual energy, this serves as a direct validation of its agreement with these known truths. Furthermore, the range-shift experiment, primarily designed to assess uncertainty, also provided a secondary validation of

agreement by confirming the framework's ability to accurately measure a final range value that corresponds to a gold-standard range shifted by a known, physical amount.

Clinical application test

Clinical feasibility tests were conducted to evaluate the practical implementation of the proposed framework. These tests included one year of long-term beam range measurements and range measurements across various gantry angles.

To evaluate long-term stability, monthly range measurements were performed from July 2023 to June 2024 in a fixed treatment room. The process involved measuring a representative subset of 100 energies, which were selected by sampling every sixth energy across all energy levels. In addition to these routine checks, comprehensive measurements of all 600 energy levels were conducted following major maintenance services in June, October, November 2023, and February 2024. For all the measurements, the determined ranges were compared with the established reference values to evaluate any deviations.

The Giraffe was securely attached to the head of the gantry head using the MLIC mount. The angular consistency was evaluated using this setup to perform range measurements for all 600 energy levels at 12 angles spaced at 30° intervals. To determine whether the beam range depended on the gantry angle, the range deviations for each angle were compared with the mean range across all 12 angles. The measurements were completed within 1 d to minimize the influence of factors other than the gantry angle.

Results

Performance of the beam-model-based fitting

A comparison of the three fitting models—Bortfeld, spline, and the proposed beam-model-based fitting method—applied to the Giraffe data, is illustrated in Fig. 3. Figs. 3(a) and 3(b) present the results for medium- (283.48 MeV/u) and low-energy (91.4 MeV/u) levels with ranges of approximately 149 mm and 15 mm, respectively.

In Fig. 3(a), which illustrates the results for the medium-energy beam (283.48 MeV/u), the Bortfeld fitting performed using OmniPro aligns well with the Giraffe data, particularly up to the second data point beyond the peak. However, it fails to account for the fragmentation tail above 151.5 mm, which leads to a noticeable discrepancy. In contrast, the beam-model-based fitting accurately captured the fragmentation tail and provided an overall curve that closely aligned with the Giraffe data points. Additionally, the range of 148.9 mm calculated using this method was close to the reference range of 149.0 mm. This high level of accuracy is not coincidental but represents a consistent trend observed across all 32 reference energies, as further detailed in the comprehensive analysis in Fig. 4. Although spline interpolation seems to match the data well in terms of intersecting the data points, it often produces substantial range value errors. Unlike beam-model-based fitting or the Bortfeld model, spline interpolation does not incorporate any physical principles or approximations related to ion–material interactions. Consequently, spline interpolation merely smoothens the curve between two data points without considering the potential singularities that may exist between them, leading to substantial errors in range determination.

The low-energy (91.4 MeV/u) results presented in Fig. 3(b) show considerable differences between the fitting models. Beam-model-based fitting accurately captured the shape of the depth-dose curve of the actual beam, showing high agreement across all data points with a determined range of 14.8 mm (reference: 14.9 mm). In contrast, Bortfeld fitting demonstrated occasional failures for carbon-ion beams, as shown in this example. These discrepancies were attributed to the fitting process being trapped at a local minimum or the failure to reproduce the characteristic shape of the ridge filter.

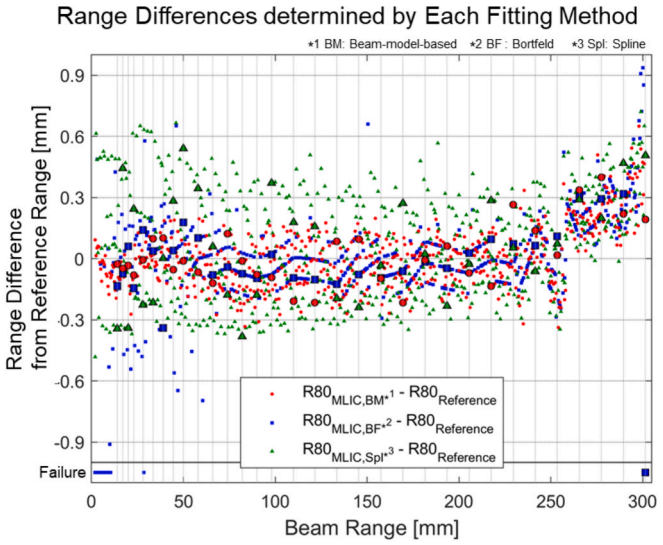

Fig. 4. Comparison of range differences for three fitting methods. Range differences from reference values for the proposed beam-model-based (BM, red circles), Bortfeld (BF, blue squares), and spline (Spl, green triangles) fitting methods. The results for the 32 reference Integral Depth Dose (IDD) energies are highlighted by large markers with black outlines, and their corresponding positions are indicated by vertical lines. The "Failure" line indicates cases where the Bortfeld fit failed to produce a valid result.

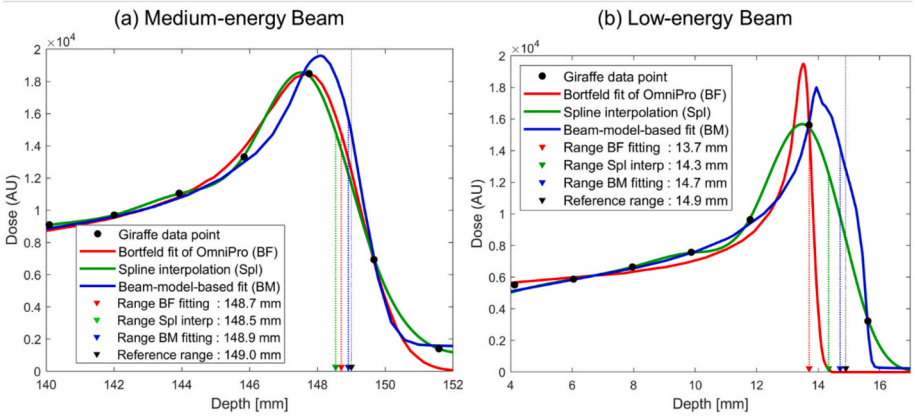

Fig. 3. Comparison of fitting methods for range analysis. (a) Medium-energy beam (reference range of 149.0 mm) and (b) low-energy beam (reference range of 14.9 mm). Bortfeld fitting on OmniPro, beam-model-based fitting, and spline interpolation curves are plotted using red, green, and blue solid lines, respectively. The downward-pointing arrows indicate the range values determined by each fitting model.

To comprehensively evaluate the performance of the three fitting methods across the entire therapeutic energy range, the differences between the ranges determined by each method and the reference ranges were analyzed, as shown in Fig. 4, which clearly highlights the limitations of conventional fitting approaches and the superiority of the proposed method in terms of reliability and uncertainty. The Bortfeld fit (blue squares) demonstrated considerable reliability issues. Although the 1 σ for the successfully fitted points was 0.19 mm, the method failed completely in 15 cases, resulting in range deviations greater than 1 mm. These failures, indicated in the figure, were predominantly observed at lower and higher beam ranges, rendering the method unsuitable for automated QA. While spline interpolation (green triangles) did not exhibit these failure types, it yielded the largest 1 σ of 0.26 mm, confirming its large measurement uncertainty across all energies. In contrast, the proposed beam-model-based fitting method (red circles) demonstrated superior performance. It achieved the lowest measurement uncertainty of 0.15 mm across all energies with no fitting failures.

Framework measurement uncertainty and agreement

The measurement uncertainty of the framework was then quantitatively evaluated using a range-shift experiment, with the results summarized in Table 1. The intrinsic standard uncertainty, $u_{intrinsic}$, of the beam-model-based fitting method was only 0.08 mm, outperforming both the Bortfeld (0.16 mm) and spline interpolation (0.21 mm) methods. The results for Bortfeld fitting were calculated only using cases where the fitting was successful in OmniPro. Cases where the fitting failed completely or resulted in incorrect fits with deviations exceeding 1.0 mm were excluded. Among the 1200 ranges measured under the four experimental conditions analyzed using OmniPro, approximately 3% (34 cases) exhibited fitting failures. In contrast, the proposed MLIC framework using beam-model-based fitting successfully determined the beam range for all energy levels provided at HITC, achieving a 100% success rate.

The agreement of the framework was evaluated by comparing its determined range for the 32 reference energies with the gold-standard values. Notably, for these energies, the framework exhibited excellent agreement with the standard QA method, yielding a mean deviation of 0.03 $\pm$ 0.15 mm (mean $\pm$ 1 σ), as highlighted by the black circles in Fig. 4. The range-shift experiment provided a secondary validation of agreement with standard QA method. As shown in Table 1, the measured range-shift (ΔR) values agreed with the standard QA method to within 0.05 mm for all slab thicknesses, confirming the framework's ability to accurately measure known, physically induced shifts.

Clinical application test

Long-term range measurements

Fig. 5(a) displays the monthly range deviations from the reference range measured over a 1-year period (July 2023–June 2024). The overall mean absolute deviation was 0.17 mm, with a maximum difference of −0.82 mm observed at a range of 264.3 mm. While the range deviation for most energies was consistently low ($\leq$ 0.14 mm), a specific region corresponding to ranges between 255 mm and 274 mm yielded a considerably higher σ of 0.41 mm. The implications of these specific deviations are examined further in the Discussion section.

Range measurements at various gantry angles

Fig. 5(b) shows the differences in the range values across the 12 gantry angles relative to the average range at each energy level. This plot highlights the consistency of measurements across different gantry angles. The maximum difference in range values across the 12 angles was 0.61 mm at a range of 257.3 mm. The overall range deviation for all energy levels across all gantry angles was 0.05 mm. Beam ranges in the range of 255–260 mm (388.71–392.84 MeV/u) exhibited a notably large deviation of 0.19 mm, whereas other ranges demonstrated a considerably lower deviation of 0.04 mm. The deviations observed in this specific range region are discussed further in the Discussion, along with the findings from long-term constancy measurements.

Discussion

The intrinsic standard uncertainty ($u_{intrinsic}$) of the proposed MLIC framework, as determined from the range-shift experiment, was 0.08 mm (1 σ). This value is notably lower than the theoretical quantization uncertainty of approximately 0.54 mm (calculated as $1.9\text{mm}/\sqrt{12}$), demonstrating that the analytical fitting effectively overcomes the discretization limit of the 1.9 mm physical channel spacing.

To establish a conservative tolerance limit for routine QA, the expanded uncertainty was calculated using a coverage factor of k = 3, yielding a value of 0.24 mm. This level of uncertainty is sufficient for verifying the beam range within the 0.5 mm interval used in the beam-range specifications. Furthermore, because the framework's range demonstrated high agreement with the reference ranges measured using the standard QA method, the proposed method is suitable for range constancy verification and obtaining reliable absolute beam range values.

The time efficiency during measurements was significantly improved. The proposed MLIC framework reduced the time for range measurements across 600 energy levels to 15 min, while the standard QA method required 50 h for the same measurements. The total measurement time was not simply 600 times the per-energy-level measurement time (0.5 s) because of the inclusion of synchrotron operation cycles, such as injection, acceleration, and deceleration. A direct comparison shows a 100-fold reduction in measurement time. While performing full-energy range measurements over 50 h (3000 min) is cumbersome, even when conducted annually, the proposed framework enables the monthly QA of beam range verification for all energy levels within a manageable workload. Additionally, the smaller size and lighter weight of the MLIC system compared with those of water phantoms reduced the setup time from 30 to 10 min, further improving operational efficiency.

The clinical application test indicated considerable variations in specific energy ranges, particularly those corresponding to values in the 255–274 mm range (388.71–406.01 MeV/u). Fig. 6(a) shows a heat map of the monthly range variations from the reference range for each beam

Table 1
Uncertainty analysis of beam-range determination using different fitting methods.

	Beam-model-based fitting		Bortfeld fitting		Spline interpolation		Standard QA method
	ΔR	u_C	ΔR	u_C	ΔR	u_C	ΔR
RW3 1 mm	1.09	0.11	1.08	0.16	1.10	0.29	1.10
RW3 2 mm	2.20	0.08	2.20	0.14	2.21	0.17	2.19
RW3 4 mm	4.33	0.10	4.33	0.22	4.33	0.25	4.28
Largest Combined Uncertainty		**0.11**		**0.22**		**0.29**	
Measurement Uncertainty($\boldsymbol{u}$)		**0.08**		**0.16**		**0.21**	
							[mm]

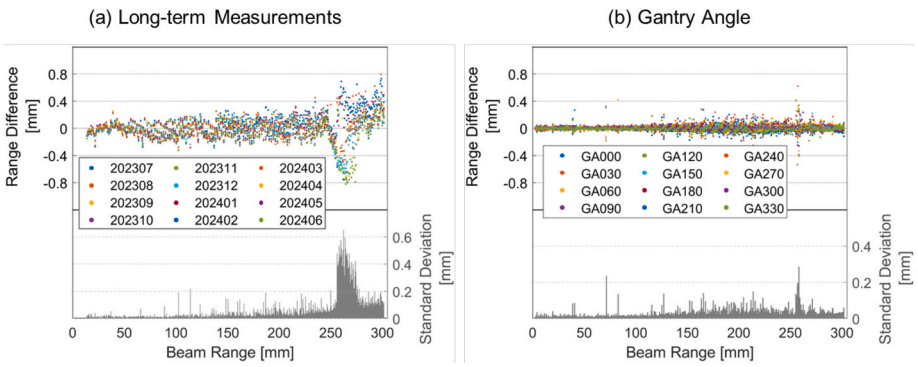

Fig. 5. Clinical application test results. (a) Monthly range differences between the measured range with the proposed framework and reference range (from July 2023 to June 2024). (b) Range differences from the gantry average across 12 angles. The upper and lower plots show the range differences and their standard deviations, respectively.

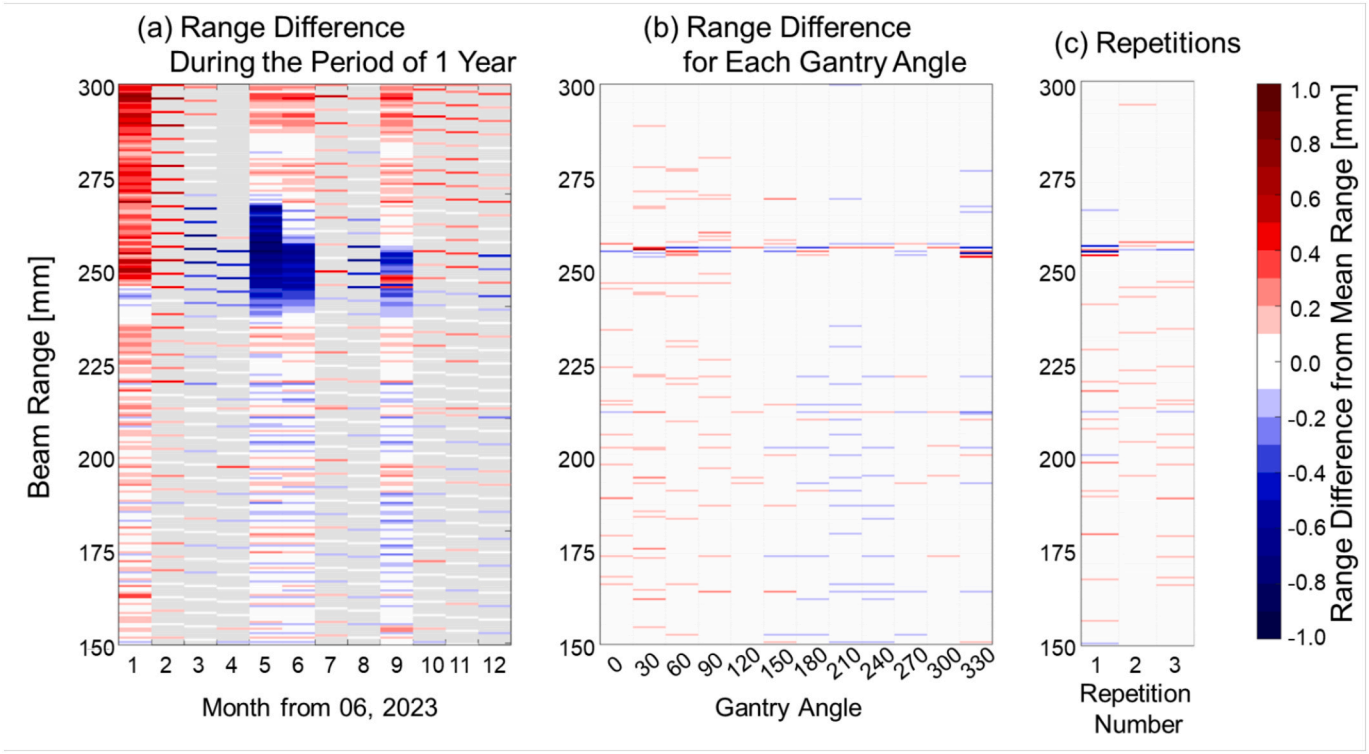

Fig. 6. Heatmap of range differences. (a) Heatmap of monthly range deviations from the reference range. (b) Heatmap of range differences relative to the mean range across 12 gantry angles. (c) Heatmap of repeated range measurements at a gantry angle of 0°.

energy. Notably, extensive beam range deviations are primarily observed in the energy range of 388.71–406.01 MeV/u. Furthermore, these deviations vary over the months. Fig. 6(b) shows the beam range deviations across different gantry angles measured within a single day. In the beam energy range of 388.71–391.01 MeV/u, noticeable variations in the beam range are observed depending on the gantry angle, whereas for other energy levels, the beam range deviations remain within the expected measurement error. Additionally, in Fig. 6(c), which shows repeated measurements at a gantry angle of 0° conducted on the same day, similarly large deviations in the specific beam energies are observed. These findings support the conclusion that the beam range fluctuations observed at specific energy levels do not indicate gantry angle dependency; instead, they result from other factors.

After the previous results were reviewed, additional experiments using the standard QA method confirmed that similar unexpected beam-range deviations were detected at specific beam energies and certain conditions. Therefore, these deviations originated from factors related to the treatment machine rather than from measurements or analysis errors. Finally, the proposed framework successfully identified machine-related issues that would have been difficult to detect using conventional methods. This enhanced detection capability can be attributed to our rapid process measuring a near-instantaneous range following a 0.1 s irradiation, whereas the standard measurement method provides an average range over a much longer data acquisition time (10–15 s), which can obscure temporal fluctuations. The existence of these deviations as an actual, machine-related issue was subsequently confirmed in collaboration with the treatment system vendor based on dedicated tests. Based on these results, an investigation request was submitted to the treatment system manufacturer, and further analysis is currently underway.

A critical consideration in this framework is the physical difference between the MLIC materials and water. As illustrated in Fig. 7, the

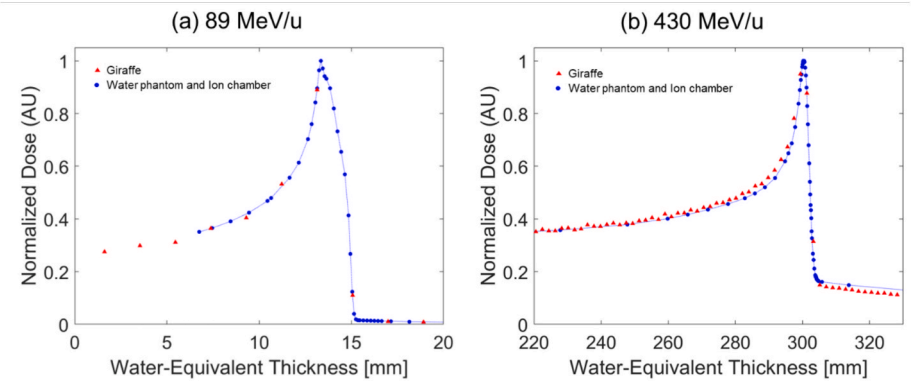

Fig. 7. Comparison of depth-dose curves measured by MLIC and water phantom. The figure shows a comparison of depth-dose curves measured with the Giraffe MLIC (red triangles) and the standard water phantom with an ion-chamber (blue circles) for (a) a low-energy (89 MeV/u) and (b) a high-energy (430 MeV/u) carbon-ion beam.

depth-dose curves measured using the Giraffe system resemble but do not perfectly match the standard water-based IDD curves. This discrepancy is energy-dependent; while the curves show relatively good agreement at low energies (89 MeV/u), a complex pattern of dose differences emerges at high energies (430 MeV/u). Unlike protons, carbon ions exhibit distinct nuclear fragmentation patterns in higher-Z materials. Consequently, the ratio of the entrance plateau to the Bragg peak is significantly affected by the detector material compared to water [22]. However, the shape of the Bragg peak itself is primarily dominated by energy straggling rather than nuclear interactions. By focusing the minimization of the Root Mean Square Deviation (RMSD) exclusively on this peak region (-8 mm to +4 mm), the water-based templates can effectively match the MLIC measurement despite the discrepancy in the Peak-to-Plateau ratio. While this selective peak-matching strategy does not serve as a physically complete depth-dose model, it provides a highly effective, data-driven optimization for routine measurement purposes. This approach serves as a robust measurement-based alternative to analytical models (e.g., Bortfeld). Unlike analytical models that attempt a universal physical description but fail to capture machine-specific modulations (e.g., the ridge filter), our template-based approach directly utilizes empirical reference data. Consequently, this strategy inherently functions as a system-specific evaluation tool, ensuring that the unique beam delivery characteristics of the specific institution are accurately reflected during routine monitoring, all while avoiding the complexity of unverified Monte Carlo simulations.

While generating intermediate templates via interpolation is a potential alternative, this study prioritized a strictly measurement-based approach using the discrete reference library. Since the Bragg peak shape evolves gradually between adjacent reference energies, the depth-shift optimization (Δd) effectively aligns the measured data with the closest reference template without requiring artificially generated intermediate shapes. Moreover, utilizing mathematical interpolation or extrapolation poses potential risks due to the complexity of carbon-ion beam optics. Theoretical modeling of energy spread variations and nuclear fragmentation, especially in the low-energy region, can be prone to uncertainties if not validated by extensive measurements. Therefore, to avoid introducing modeling artifacts or user-dependent biases, we deliberately excluded curve generation techniques. This strategy ensures that the range determination remains entirely grounded in verified physical measurements, thereby maximizing the robustness and reliability of the framework.

Despite the significant efficiency improvements achieved with the proposed framework, which enables range determination comparable to the standard QA method, it is designed to function as a high-frequency monitoring tool that complements, rather than completely replaces, the standard method. This framework relies on pragmatic peak-matching tailored for routine measurement purposes, rather than providing a universally applicable, physically complete depth-dose modeling. This limitation is primarily attributed to the necessity of an initial spatial cross-calibration. To ensure accurate range determination, the effective water-equivalent path length of the MLIC's absorber stack must be benchmarked against reference IDD measurements obtained using the standard water-phantom method. Consequently, the framework relies on the standard method for this one-time initialization to establish a baseline. However, once this spatial baseline is established, the framework allows for independent, routine monitoring of beam range fluctuations. Furthermore, the standard method remains indispensable for generating the pristine IDD data required for TPS beam modeling. As described in the Methods section, TPS beam modeling necessitates IDD data with high-depth resolution. The MLIC system, with a 2 mm depth resolution per channel, cannot capture the detailed dose gradients achieved by the water-phantom-based standard method, which allows measurement intervals as small as 0.1 mm (Fig. 7).

To address these limitations, future research will explore a new analytical Bragg curve approximation model for carbon ions that combines the universal applicability of the Bortfeld equation with the capacity to integrate machine-specific modulations. Developing such a model—one capable of simultaneously accounting for generalized physical interactions and system-specific beam delivery characteristics—will not only yield superior fitting accuracy for conventional measurement methods but also serve as a crucial next step in deriving accurate, water-equivalent IDDs directly from MLIC measurements.

Conclusion

In this study, we developed and validated an efficient framework using an MLIC to overcome the significant time and logistical constraints of routine beam-range QA in carbon-ion radiotherapy. By integrating a carbon-ion-specific beam-model-based fitting method, a gantry-compatible mount, and a time-optimized acquisition process, our framework provides a comprehensive solution for frequent and multi-angle QA.

The framework demonstrated low uncertainty, with an expanded uncertainty of 0.24 mm (k = 3), and excellent agreement with gold-standard reference measurements (mean deviation of 0.03 ± 0.15 mm). Most notably, it reduced the measurement time for all 600 energies from >50 h to just 15 min. This significant efficiency improvement enabled comprehensive routine monitoring, which led to the identification of previously undetectable machine-related range deviations. Rather than claiming universal applicability for carbon-ion depth-dose characterization, the agreement observed between the water-based templates and MLIC measurements demonstrates a highly effective, system-specific evaluation strategy tailored for practical QA.

However, it must be emphasized that this framework is designed as a

powerful tool for routine QA. It does not replace the indispensable role of the standard water phantom method for initial commissioning and the establishment of the reference IDD data upon which our model relies.

In conclusion, the proposed MLIC framework serves as a practical, measurement-driven tool for carbon-ion beam range verification with low uncertainty. The use of empirical reference data allows this approach to effectively account for system-specific beam delivery characteristics and modulations. Consequently, the optimized and streamlined workflow facilitates routine clinical QA across all energy levels and gantry angles.

Statement of Ethics

No ethics approval was required for the report, and no human participants were involved.

CRediT authorship contribution statement

Soorim Han: Writing – original draft, Visualization, Validation, Software, Methodology, Investigation, Data curation, Conceptualization. **YongCheol Kwon:** Software, Data curation. **Taegeon Oh:** Validation, Data curation. **Eunho Lee:** Validation, Data curation. **Eun Kyu Kim:** Validation, Data curation. **Tae Ho Kim:** Validation, Methodology, Data curation. **Dohyeon Yoo:** Validation, Data curation. **Sangmin Lee:** Validation, Data curation. **Changhwan Kim:** Writing – review & editing, Validation, Supervision, Formal analysis. **Min Cheol Han:** Writing – review & editing, Validation, Supervision, Resources. **Chae-Seon Hong:** Writing – review & editing, Validation, Resources, Project administration. **Jin Sung Kim:** Supervision, Resources, Project administration, Funding acquisition.

Funding

This study was supported by a faculty research grant from Yonsei University College of Medicine (6-2023-00107) and by the Basic Science Research Program through the National Research Foundation of Korea, funded by the Ministry of Education (grant number 2022R1I1A1A01068163).

Declaration of competing interest

The authors declare that they have no known competing financial interests or personal relationships that could have appeared to influence the work reported in this paper.

Acknowledgments

We express our sincere gratitude to the Yonsei University Health System for granting us permission to conduct this study. We thank the medical physicists for their invaluable assistance in measurements and operational support, as well as the dedicated individuals at the Department of Radiation Oncology, including professors, fellows, and administrative staff, for their unwavering commitment and support.

Declaration of Generative AI and AI-assisted Technologies in the Writing Process

During the preparation of this work, the authors used Google Gemini in order to improve readability. After using this tool/service, the authors reviewed and edited the content as needed and take full responsibility for the content of the publication.

References

[1] Byun HK, Han MC, Yang K, Kim JS, Yoo GS, Koom WS, et al. Physical and Biological Characteristics of Particle Therapy for Oncologists. Cancer Res Treat. 2021;53:611–20.
[2] Thariat J, Hannoun-Levi JM, Sun Myint A, Vuong T, Gerard JP. Past, present, and future of radiotherapy for the benefit of patients. Nat Rev Clin Oncol. 2013;10:52–60.
[3] Tsujii H, Kamada T, Shirai T, Noda K, Tsuji H, Carbon-Ion KK, et al. Planning 2014.
[4] Thasasi P, Ruangchan S, Oonsiri P, Oonsiri S. Determination of Integral Depth Dose in Proton Pencil Beam Using Plane-parallel Ionization Chambers. Int J Part Ther. 2022;9:1–9.
[5] Decabooter E, Roijen E, Martens J, Unipan M, Bosmans G, Vilches-Freixas G. Quality assurance of scanned proton beams at different gantry angles using an ionization chamber array in a rotational phantom. Phys Med. 2022;104:67–74.
[6] Rana S, Eckert C, Tesfamicael B. Feasibility study of utilizing Sphinx Compact for quality assurance in uniform scanning proton therapy. Phys Med. 2023;113:102468.
[7] Shimbo M, Urakabe E, Futami Y, Yusa K, Yamashita H, Matsufuji N, et al. Development of a multi-layer ion chamber for measurement of depth dose distributions of heavy-ion therapeutic beam for individual patients. Nihon Igaku Hoshasen Gakkai Zasshi. 2000;60:274–9.
[8] Farace P, Righetto R, Meijers A. Pencil beam proton radiography using a multilayer ionization chamber. Phys Med Biol. 2016;61:4078–87.
[9] Vai A, Mirandola A, Magro G, Maestri D, Mastella E, Mairani A, et al. Characterization of a MLIC Detector for QA in Scanned Proton and Carbon Ion Beams. Int J Part Ther. 2019;6:50–9.
[10] Bortfeld T. An analytical approximation of the Bragg curve for therapeutic proton beams. Med Phys. 1997;24:2024–33.
[11] Schwaab J, Brons S, Fieres J, Parodi K. Experimental characterization of lateral profiles of scanned proton and carbon ion pencil beams for improved beam models in ion therapy treatment planning. Phys Med Biol. 2011;56:7813–27.
[12] Han MC, Choi SH, Hong CS, Kim YB, Koom WS, Kim JS, et al. The first Korean carbon-ion radiation therapy facility: current status of the Heavy-ion Therapy Center at the Yonsei Cancer Center. Radiat Oncol J. 2024;42:295–307.
[13] Furukawa T, Hara Y, Mizushima K, Saotome N, Tansho R, Saraya Y, et al. Development of NIRS pencil beam scanning system for carbon ion radiotherapy. Nucl Instrum Meth B. 2017;406:361–7.
[14] Haberer T, Becher W, Schardt D, Kraft G. Magnetic Scanning System for Heavy-Ion Therapy. Nucl Instrum Meth A. 1993;330:296–305.
[15] Furukawa T, Inaniwa T, Sato S, Shirai T, Takei Y, Takeshita E, et al. Performance of the NIRS fast scanning system for heavy-ion radiotherapy. Med Phys. 2010;37:5672–82.
[16] Iwata Y, Kadowaki T, Uchiyama H, Fujimoto T, Takada E, Shirai T, et al. Multiple-energy operation with extended flattops at HIMAC, Nuclear Instruments and Methods in Physics Research Section A: Accelerators. Spectrometers, Detectors and Associated Equipment. 2010;624:33–8.
[17] Schuemann J, Dowdell S, Grassberger C, Min CH, Paganetti H. Site-specific range uncertainties caused by dose calculation algorithms for proton therapy. Phys Med Biol. 2014;59:4007–31.
[18] Hara Y, Furukawa T, Inaniwa T, Mizushima K, Shirai T, Noda K. A novel method for experimental characterization of large-angle scattered particles in scanned carbon-ion therapy. Med Phys. 2014;41:021706.
[19] Clasie B, Depauw N, Fransen M, Goma C, Panahandeh HR, Seco J, et al. Golden beam data for proton pencil-beam scanning. Phys Med Biol. 2012;57:1147–58.
[20] Dhanesar S, Sahoo N, Kerr M, Taylor MB, Summers P, Zhu XR, et al. Quality assurance of proton beams using a multilayer ionization chamber system. Med Phys. 2013;40:092102.
[21] Jakel O. Physical advantages of particles: protons and light ions. Br J Radiol. 2020;93:20190428.
[22] Yajima K, Kanai T, Kusano Y, Shimojyu T. Development of a multi-layer ionization chamber for heavy-ion radiotherapy. Phys Med Biol. 2009;54:N107–14.